

Move What Matters: Parameter-Efficient Domain Adaptation via Optimal Transport Flow for Collaborative Perception

Zesheng Jia¹ Jin Wang^{1*} Siao Liu^{1*} Lingzhi Li¹ Ziyao Huang² Yunjiang Xu² Jianping Wang²

¹School of Future Science and Engineering, Soochow University

²City University of Hong Kong

Abstract

Fast domain adaptation remains a fundamental challenge for deploying multi-agent systems across diverse environments in Vehicle-to-Everything (V2X) collaborative perception. Despite the success of Parameter-Efficient Fine-Tuning (PEFT) in natural language processing and conventional vision tasks, directly applying PEFT to multi-agent settings leads to significant performance degradation and training instability. In this work, we conduct a detailed analysis and identify two key factors: (i) inter-frame redundancy in heterogeneous sensory streams, and (ii) erosion of fine-grained semantics in deep-layer representations under PEFT adaptation. To address these issues, we propose FlowAdapt, a parameter-efficient framework grounded in optimal transport theory, which minimizes information transport costs across both data distributions and network hierarchies. Specifically, we introduce a Wasserstein Greedy Sampling strategy to selectively filter redundant samples via a bounded covering radius. Furthermore, Progressive Knowledge Transfer module is designed to progressively inject compressed early-stage representations into later stages through learnable pathways, alleviating semantic degradation in late-stage adaptation. Extensive experiments on three benchmarks demonstrate that FlowAdapt achieves state-of-the-art performance with only 1% of trainable parameters, effectively bridging domain gaps with superior sample efficiency and generalization.

1. Introduction

Autonomous vehicles suffer from inherent perceptual limitations including occlusions, restricted field-of-view, and limited sensing range [2, 18, 48]. Vehicle-to-Everything (V2X) collaborative perception bridges the gap between isolated single-agent observation and comprehensive environmental awareness through multi-agent information sharing [3, 31, 36, 50]. Existing collaborative perception methods predominantly assume that training and deployment

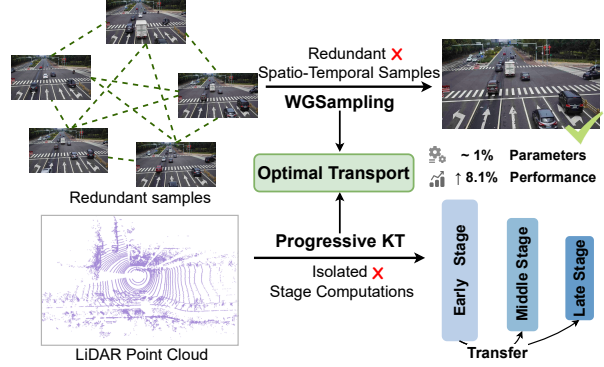


Figure 1. FlowAdapt tackles dual challenges in collaborative perception adaptation: eliminating redundant spatio-temporal samples through Wasserstein greedy sampling, and bridging isolated stage computations through progressive knowledge distillation.

data remain consistent in sensor configurations and environmental conditions [39]. This assumption rarely holds in practice, where training and deployment domains typically diverge in sensor modalities and environmental conditions. However, developing domain-specific models or retraining from scratch would incur prohibitive computational and annotation costs [32], which makes efficient cross-domain adaptation a critical challenge for collaborative perception.

To overcome this limitation, parameter-efficient fine-tuning (PEFT) offers a promising solution by updating only a small fraction of model parameters while maintaining performance. PEFT methods such as adapters [15] and LoRA [16] have demonstrated success in natural language processing and single-agent vision tasks [14, 41], significantly reducing training costs compared to full fine-tuning. Building on these advances, recent works introduce PEFT to collaborative perception. MACP [32] freezes pre-trained backbones and inserts lightweight modules for multi-agent collaboration. CoPEFT [39] further proposes Collaboration Adapter and Agent Prompt for hierarchical adaptation with limited trainable parameters. Despite substantial progress, existing PEFT-based approaches [32, 39] still exhibit a nontrivial performance gap. Therefore, we conduct

*Corresponding authors: wjin1985@suda.edu.cn; saliu@suda.edu.cn

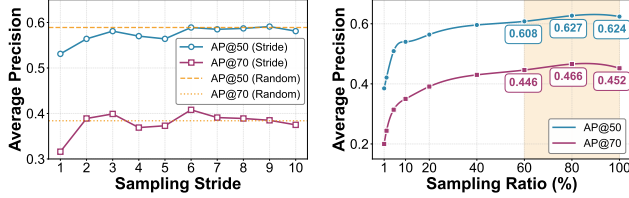


Figure 2. **Left:** Performance versus temporal stride (interval between consecutively selected frames) with fixed 10% sampling ratio. **Right:** Performance vs. sampling ratio with sequential selection. Performance saturates beyond 60% (orange-shaded zone).

a systematic analysis of the state-of-the-art PEFT method, CoPEFT [39], and identify two critical phenomena that hinder effective adaptation: (i) **Inter-frame redundancy** across heterogeneous sensory streams. As illustrated in Figure 2, training on a subset of training frames can even exceed full-sequence performance, and average precision saturates beyond a 60% sampling ratio. (ii) PEFT-induced **semantic erosion** in the deep layers. Figure 3 reveals that fine-grained semantics attenuate along the hierarchy in PEFT-based models, whereas the enhanced late-layer representations can substantially recover semantic richness.

In this work, we rethink fast domain adaptation for collaborative perception from an information-theoretic perspective. We argue that PEFT in multi-agent settings can be viewed as an optimal transport problem, which aims to seek an efficient shortcut that carries task-relevant mass from source to target domains with minimal trainable parameters. Under this hypothesis, inter-frame redundancy represents low-value information mass that should be filtered, while semantic erosion under PEFT arises from deteriorated information transport across network layers, causing premature loss of fine-grained semantics in deeper layers.

Based on these insights, we propose FlowAdapt, the first parameter-efficient framework to unify sample selection and cross-stage knowledge transfer under the optimal transport [34] paradigm for collaborative perception adaptation. In particular, FlowAdapt achieves efficient information transport through two key components: Wasserstein Greedy Sampling (WGS) and Progressive Knowledge Transfer (KTPro). As illustrated in Figure 1, WGS reformulates sample redundancy as identifying a minimum dominating set in spatio-temporal feature space with bounded covering radius, using Wasserstein distance to eliminate redundant samples while preserving distribution coverage. Meanwhile, KTPro addresses semantic erosion by compressing early-stage representations and progressively injecting them into later stages via learnable pathways, establishing efficient shortcuts that transport fine-grained semantics directly to later layers. We conduct extensive experiments on three collaborative perception benchmarks, achieving state-of-the-art adaptation performance with exceptional parameter efficiency and generalization. In sum-

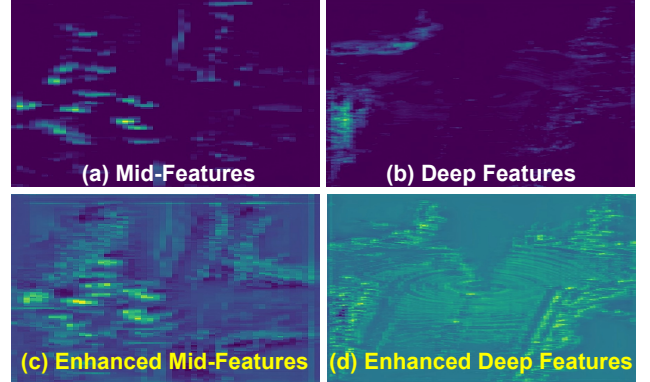


Figure 3. We extract feature visualizations at three network depths during adaptation: shallow (after voxelization), middle (backbone intermediate), and deep (before detection head). (a-b) show sparse activation in middle and deep layers. (c-d) show middle and deep layer visualizations after injecting compressed shallow features.

mary, our contribution encompasses three main manifolds:

- We perform systematic ablations and identify two key factors that impede PEFT in collaborative perception: **inter-frame redundancy** and **semantic erosion** in deep layers, providing principled insights for optimizing information flow across both data and network hierarchies.
- We propose FlowAdapt, a parameter-efficient framework that formulates collaborative perception adaptation as an optimal transport problem. WGS eliminates spatio-temporal redundancy via minimum dominating set formulation, while KTPro effectively recovers semantic information through learnable cross-stage pathways.
- Extensive experiments on three benchmarks demonstrate that FlowAdapt achieves SOTA performance with only 1% trainable parameters and superior generalization.

2. Related Work

2.1. Collaborative Perception

Collaborative perception enables information exchange among cooperative agents to expand sensing coverage beyond individual vehicle constraints [3, 23, 26]. Early approaches adopted early fusion via raw sensory data [4] or late fusion via detection outputs [35]. Recent works primarily explore intermediate fusion [3, 38, 43, 47] balancing accuracy and bandwidth efficiency. V2X-ViT [44, 46] employs Transformers to address asynchronous sharing and pose errors. To optimize communication-performance trade-offs, Who2com [29], When2com [28], and Where2comm [17] selectively determine communication strategies. CoAlign [30] and FreeAlign [21] improve pose error robustness through agent-object pose graphs and geometric pattern recognition. Recent works address heterogeneity and uncertainties: HEAL [31] handles sensor heterogeneity, ERMVP [50] tackles bandwidth and localization uncertainties, and TraF-Align [36] addresses inter-

agent latency. Despite these advances, existing methods assume consistent training-deployment distributions, neglecting domain shifts and efficient adaptation needs.

2.2. Parameter-Efficient Fine-Tuning

Parameter-efficient fine-tuning (PEFT) has emerged as a scalable alternative to full fine-tuning for adapting pre-trained models [13, 24]. Representative methods include: Adapter [15] inserts trainable bottleneck layers between frozen transformer blocks, LoRA [16] and its variants [9, 27, 51] decompose weight updates into low-rank matrices, and Prefix-Tuning [22] optimizes learnable prompts prepended to inputs. Recent vision works [5, 19] demonstrate PEFT can outperform full fine-tuning on vision transformers with less than 2% trainable parameters. In collaborative perception, MACP [32] freezes pre-trained backbones and adds lightweight collaborative modules, while CoPEFT [39] proposes Collaboration Adapter and Agent Prompt for hierarchical adaptation. We adopt cross-stage knowledge transfer to bridge network stages, achieving more efficient adaptation for collaborative perception.

2.3. Optimal Transport

Optimal transport theory provides a principled framework for efficient distribution alignment [7, 34]. Courty et al. [6] employ it for domain adaptation by aligning distributions while preserving semantic structures. Arjovsky et al. [1] demonstrate Wasserstein distance stabilizes GAN training by providing meaningful gradients even with disjoint distributions. Recent works extend it to model training: GORACS [33] formulates coresnet selection as minimizing transport costs to identify subsets that align with fine-tuning objectives, while Multi-Level OT [8] employs Wasserstein distance for cross-architecture knowledge distillation. Following this principle, we formulate sample selection as identifying a minimum dominating set in spatio-temporal feature space via Wasserstein distance, ensuring distribution coverage with provable guarantees.

3. Method

3.1. Problem Definition

In collaborative perception for V2X systems, N connected autonomous vehicles collaborate to perform 3D object detection. A critical challenge arises when deploying pre-trained models from source domain \mathcal{D}_s to target domains \mathcal{D}_t : distribution shifts caused by varying traffic patterns or environmental conditions significantly degrade detection accuracy, while full model retraining incurs prohibitive computational costs for resource-constrained systems.

We formulate the parameter-efficient adaptation problem: Given a pre-trained collaborative detection model f_Θ with parameters Θ and limited labeled samples from target domain $\mathcal{D}_t^{few} = \{(\mathcal{O}_i^t, \mathcal{B}_i^t)\}_{i=1}^K$ where $K \ll |\mathcal{D}_s|$, the ob-

jective is to adapt the model by updating only a minimal parameter subset $\Delta\Theta$ with $|\Delta\Theta| \ll |\Theta|$:

$$\min_{\Delta\Theta} \mathcal{L}_{det}(f_{\Theta+\Delta\Theta}, \mathcal{D}_t^{few}) + \lambda \cdot |\Delta\Theta|, \quad (1)$$

where \mathcal{L}_{det} denotes the detection loss and λ controls parameter efficiency. This enables effective target domain adaptation while maintaining minimal trainable parameters.

3.2. Overall Architecture

The overall Architecture are shown in the Figure 4. Consider N collaborative agents $\mathcal{A} = \{A_1, \dots, A_N\}$ in a cooperative perception environment, where each agent A_i is equipped with LiDAR sensor providing observation \mathcal{O}_i . Given target domain dataset \mathcal{D} and sampling ratio $\alpha \in (0, 1]$, Wasserstein Greedy Sampling (WGS) identifies a representative subset $\mathcal{D}_s \subseteq \mathcal{D}$ with $|\mathcal{D}_s| = \lfloor \alpha |\mathcal{D}| \rfloor$ through greedy selection guided by weighted Wasserstein distance. The processing pipeline for agent A_i can be denoted as:

$$\mathcal{D}_s = \text{WGS}(\mathcal{D}, \alpha), \quad (2a)$$

$$\mathcal{F}_i = f_{\text{enc}}(\mathcal{O}_i), \quad \hat{\mathcal{F}}_i, \mathcal{P}_i = f_{\text{adapt}}^{\text{early}}(\mathcal{F}_i), \quad (2b)$$

$$\mathcal{F}_{j \rightarrow i} = \Gamma_{j \rightarrow i}(\hat{\mathcal{F}}_j), \quad \mathcal{P}_{j \rightarrow i} = \Gamma_{j \rightarrow i}(\mathcal{P}_j), \quad (2c)$$

$$\mathcal{H}_i = f_{\text{fus}}(\{\mathcal{F}_{j \rightarrow i}\}_{j=1}^N, \{\mathcal{P}_{j \rightarrow i}\}_{j=1}^N), \quad (2d)$$

$$\hat{\mathcal{H}}_i = f_{\text{adapt}}^{\text{late}}(\mathcal{H}_i, \mathcal{M}_{\text{early}}), \quad \mathcal{B}_i = f_{\text{det}}(\hat{\mathcal{H}}_i), \quad (2e)$$

where the frozen encoder f_{enc} are used for extracting BEV features \mathcal{F}_i from observations. For each agent, early-stage adaptation $f_{\text{adapt}}^{\text{early}}$ generates adapted features $\hat{\mathcal{F}}_i$ and agent prompts \mathcal{P}_i via dual-path processing intra-group aggregation, caching features in $\mathcal{M}_{\text{early}}$ for cross-stage transfer. We utilize a spatial transformation $\Gamma_{j \rightarrow i}$ aligns features and prompts to ego coordinates. Besides, a fusion module f_{fus} aggregates aligned information into collaborative representation \mathcal{H}_i . During the late-stage adaptation, $f_{\text{adapt}}^{\text{late}}$ injects compressed knowledge from $\mathcal{M}_{\text{early}}$ to produce refined features $\hat{\mathcal{H}}_i$. Detection head f_{det} generates final predictions \mathcal{B}_i .

3.3. Wasserstein Greedy Sampling

In collaborative perception adaptation, substantial redundancy that exists in multi-agent sensory streams severely impedes efficient fine-tuning and rapid deployment. Therefore, we propose Wasserstein Greedy Sampling (WGS), aiming to achieve optimal data coverage for adaptation through principled selection that minimizes redundancy while preserving critical spatio-temporal diversity.

Feature Representation and Metric Design. We construct a feature space $\mathcal{F} \subseteq \mathbb{R}^4$ that encodes the spatio-temporal dynamics critical to cooperative perception. Given a dataset $\mathcal{D} = \{(x_i, t_i, p_i)\}_{i=1}^n$ with sensory observation x_i , timestamp t_i , and spatial configuration $p_i \in \mathbb{R}^3$, we extract a feature vector $\mathbf{f}_i = [f_i^t, f_i^x, f_i^y, f_i^s]^\top \in \mathcal{F}$ where: $f_i^t = t_i/\tau$

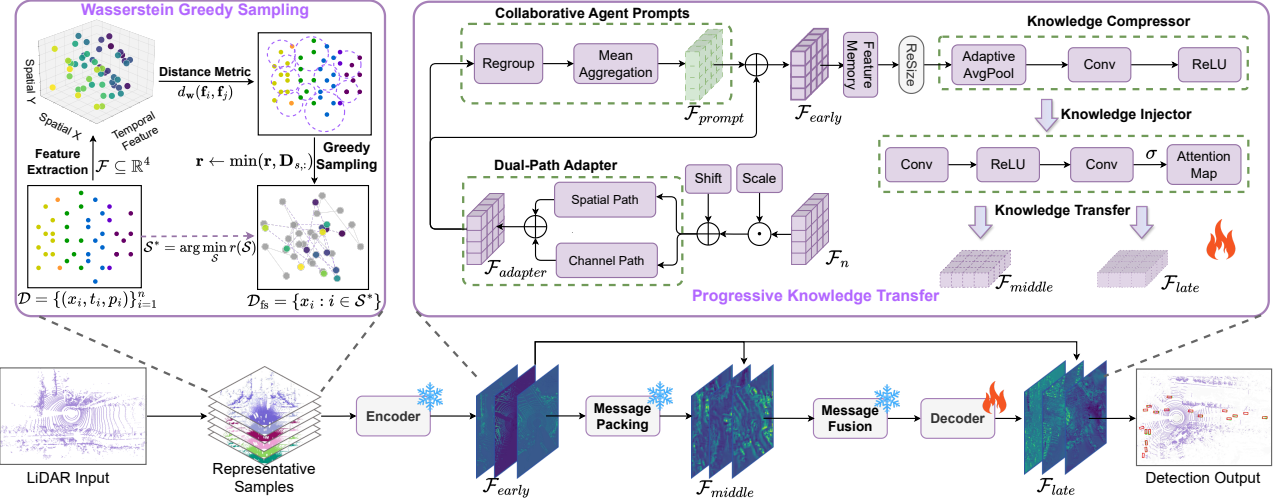


Figure 4. Overview of FlowAdapt. Wasserstein Greedy Sampling selects representative samples by minimizing coverage radius in spatio-temporal feature space. Progressive Knowledge Transfer operates across network stages: Collaborative Agent Prompts and Dual-Path Adapters enhance feature representations through intra-group aggregation and complementary spatial-channel processing, while the compression-injection mechanism transfers early-stage knowledge to later stages to mitigate semantic erosion.

(temporal normalization with $\tau = 10^6$), $(f_i^x, f_i^y) = \phi(p_i)$ (spatial projection $\phi : \mathbb{R}^3 \rightarrow [-1, 1]^2$), and $f_i^s = i/n$ (normalized sequential position). Building upon this feature representation, we design a Wasserstein-inspired distance metric that quantifies sample dissimilarity:

$$d_w(\mathbf{f}_i, \mathbf{f}_j) = \left(\sum_{k \in \{t, x, y, s\}} w_k (f_i^k - f_j^k)^2 \right)^{1/2}, \quad (3)$$

with weight vector $\mathbf{w} = [2.0, 1.0, 1.0, 0.5]^\top$ prioritizing temporal diversity for capturing dynamic scene evolution, followed by spatial coverage for viewpoint comprehensiveness, and sequential ordering for data coherence.

Optimal Transport Formulation. We reformulate data selection as an optimal transport problem between empirical distributions. Let $\mu_n = \frac{1}{n} \sum_{i=1}^n \delta_{\mathbf{f}_i}$ denote the empirical distribution of the full dataset and $\nu_m = \frac{1}{m} \sum_{j \in \mathcal{S}} \delta_{\mathbf{f}_j}$ represent the distribution of the selected subset \mathcal{S} , where $\delta_{\mathbf{f}}$ is the Dirac measure at \mathbf{f} . The Wasserstein distance between these distributions is defined as:

$$W_p(\mu_n, \nu_m) = \left(\inf_{\gamma \in \Gamma(\mu_n, \nu_m)} \int d_w(\mathbf{f}, \mathbf{f}')^p d\gamma(\mathbf{f}, \mathbf{f}') \right)^{1/p}, \quad (4)$$

where $\Gamma(\mu_n, \nu_m)$ denotes the set of all couplings (joint distributions) with marginals μ_n and ν_m . However, directly minimizing $W_p(\mu_n, \nu_m)$ is computationally intractable for large-scale datasets. Instead, we adopt a coverage-based proxy that minimizes the maximum transport cost:

$$\mathcal{S}^* = \arg \min_{\mathcal{S} \subseteq \mathcal{D}} \max_{|\mathcal{S}|=m} \min_{\mathbf{f}_i \in \mathcal{F}} \min_{\mathbf{f}_j \in \mathcal{F}_{\mathcal{S}}} d_w(\mathbf{f}_i, \mathbf{f}_j). \quad (5)$$

This formulation ensures every point in the original distribution has a representative in the selected subset within bounded transport cost, constructing a Wasserstein ball of minimal radius that covers the entire feature space. Algorithm 1 details the complete procedure.

Theorem. In the metric space (\mathcal{F}, d_w) , farthest-first WGS returns an m -point subset \mathcal{S}_{WGS} whose coverage radius satisfies $R(\mathcal{S}_{WGS}) \leq 2R^*$, where R^* is the k -center radius.

Proof sketch. By the classical González argument [11], consider the Voronoi partition of an optimal solution \mathcal{S}^* with m centers. Since WGS selects m centers, two greedy centers could lie in one optimal cell, the farthest-first rule bounds their distance by $2R^*$. Assign every point to its nearest greedy center; by the triangle inequality within that cell, each point is within $2R^*$ greedy center, which upper bounds the greedy radius. Full proof refer to the **Appendix**.

Remark 1 A perspective from OT. For uniform empirical measures $\mu_n = \frac{1}{n} \sum_i \delta_{\mathbf{f}_i}$ and $\nu_m = \frac{1}{m} \sum_{j \in \mathcal{S}_{WGS}} \delta_{\mathbf{f}_j}$, the coverage radius controls worst-case transport:

$$W_\infty(\mu_n, \nu_m) \leq R(\mathcal{S}_{WGS}) \leq 2R^*.$$

Thus WGS builds a minimal-radius qasserstein ball that preserves distributional support under aggressive sampling.

Remark 2 Ground metric & stability. With weights \mathbf{w} , the weighted ℓ_2 ground metric d_w is a valid metric, so the 2-approximation bound applies. Larger w_t promotes temporal spread and (w_x, w_y) could promote spatial coverage.

3.4. Progressive Knowledge Transfer

Shallow layers preserve rich spatial details, while deeper layers focus on semantic abstraction but suffer from information loss during forward propagation—as observed in

Algorithm 1 Wasserstein Greedy Sampling

Input: Dataset $\mathcal{D} = \{(x_i, t_i, p_i)\}_{i=1}^n$; Selection rate $\alpha \in (0, 1]$; Weight vector $\mathbf{w} \in \mathbb{R}^4$
Output: Selected subset \mathcal{S} with $|\mathcal{S}| = m$

```

1  function WGS( $\mathcal{D}, \alpha, \mathbf{w}$ )
2   $n \leftarrow |\mathcal{D}|, m \leftarrow \lfloor \alpha n \rfloor$ 
3   $\mathbf{F} \leftarrow \text{ExtractFeatures}(\mathcal{D})$ 
4  for  $i, j \in \{1, \dots, n\}$  do            $\triangleright$  Pairwise distances
5     $\mathbf{D}_{ij} \leftarrow \sqrt{\sum_k w_k (f_i^k - f_j^k)^2}$ 
6  end for
7   $\boldsymbol{\mu} \leftarrow \frac{1}{n} \sum_j \mathbf{D}_{:,j}$             $\triangleright$  Initialize with medoid
8   $s_1 \leftarrow \arg \min_i |\mu_i - \text{median}(\boldsymbol{\mu})|$ 
9   $\mathcal{S} \leftarrow \{s_1\}$ 
10  $\mathbf{r} \leftarrow \mathbf{D}_{s_1,:}$             $\triangleright$  Coverage radio
11 while  $|\mathcal{S}| < m$  do            $\triangleright$  Iterative expansion
12    $s^* \leftarrow \arg \max_{i \notin \mathcal{S}} r_i$ 
13    $\mathcal{S} \leftarrow \mathcal{S} \cup \{s^*\}$ 
14    $\mathbf{r} \leftarrow \min(\mathbf{r}, \mathbf{D}_{s^*,:})$ 
15 end while
16 return  $\{(x_i, t_i, p_i) : i \in \mathcal{S}\}$ 
17 end function

```

Figure 3. To address this semantic erosion, we propose Progressive Knowledge Transfer (KTPro), which formulates cross-stage adaptation as an optimal transport problem. KTPro establishes efficient pathways that transfer compressed early-stage representations directly to later stages, enabling them to benefit from preserved spatial information while minimizing transport cost across network hierarchies. We define three stages: the *early stage* produces features after voxelization (before the backbone), the *middle stage* generates intermediate representations within the backbone, and the *late stage* outputs final features (before detection).

Cross-Stage Knowledge Transfer Mechanism. The core innovation lies in establishing efficient knowledge pathways across non-adjacent network stages. Unlike conventional approaches requiring feature dimension alignment, we design a compression-injection mechanism that adaptively transfers knowledge between heterogeneous stages while preserving essential information. Our transfer operates in two phases. First, a *knowledge compressor* distills early-stage features into compact representations:

$$\begin{aligned} \mathcal{K}_c &= \phi_{\text{compress}}(\mathcal{F}_{\text{early}}) \\ &= \text{ReLU}(\text{BN}(\text{Conv}(\text{Pool}(\mathcal{F}_{\text{early}})))) \end{aligned} \quad (6)$$

where compression ratio r creates an information bottleneck, forcing the network to extract discriminative patterns. The compressed \mathcal{K}_c serves as a compact knowledge carrier efficiently transported to deeper stages. Then, we utilize *knowledge injector* to transform compressed early representations via a stage-specific attention operation:

$$\mathcal{A} = \sigma(\text{Conv}(\text{ReLU}(\text{BN}(\text{Conv}(\mathcal{K}_c))))) \quad (7)$$

where $\sigma(\cdot)$ denotes sigmoid activation. This attention map enhances later-stage features through multiplicative gating:

$$\mathcal{F}_{\text{enhanced}} = \mathcal{F}_{\text{later}} \odot (1 + \alpha \cdot \mathcal{A}), \quad (8)$$

where $\alpha \in [0.1, 0.5]$ is a learnable coefficient and \odot denotes element-wise multiplication. This design selectively amplifies essential spatial patterns from early stages while suppressing redundant information in deeper representations.

Stage-Aware Capacity Allocation. To balance adaptation capability and efficiency, we adopt progressive capacity reduction across stages. The compression ratio r increases with network depth ($r_{\text{early}} < r_{\text{middle}} < r_{\text{late}}$), reflecting that early stages require higher capacity for raw feature adaptation while later stages leverage transferred knowledge with fewer parameters. The number of adaptation blocks follows similar progression: $N_{\text{early}} = 3$ for capturing complex patterns, while $N_{\text{middle}} = N_{\text{late}} = 1$ for lightweight refinement. This hierarchical allocation reduces overall transport cost and later stages can receive pre-processed compression features and perform only domain-specific adjustments.

Decoupled Feature Memory. For efficient cross-stage routing with stabilized optimization dynamics, we employ a lightweight decoupled feature memory as follows:

$$\mathcal{M}_{\text{early}} = \text{detach}(\mathcal{F}_{\text{early}}^{\text{adapted}}). \quad (9)$$

The detachment operation prevents gradient backpropagation through the memory module, avoiding memory overhead from maintaining extended computation graphs. Later stages directly access $\mathcal{M}_{\text{early}}$ for knowledge injection (Eq. 8), ensuring stable gradient computation.

3.5. Key Design Decisions

Dual-Path Adapter Architecture. To effectively capture both spatial and semantic characteristics essential for multi-agent collaboration, we design a dual-path adapter that processes features through complementary pathways. The *spatial path* employs grouped convolutions to capture local geometric patterns critical for handling diverse agent viewpoints, while the *channel path* models global semantic dependencies through point-wise projections. These pathways are dynamically fused via learnable weights:

$$\mathcal{A}(\mathcal{F}) = w_s \cdot \mathcal{A}_{\text{spatial}}(\mathcal{F}) + w_c \cdot \mathcal{A}_{\text{channel}}(\mathcal{F}), \quad (10)$$

where w_s, w_c are softmax-normalized fusion coefficients that adaptively balance spatial and channel emphasis based on corresponding feature characteristics.

Collaborative Agent Prompts. While dual-path adapters provide global feature adaptation, multi-agent systems require agent-specific refinement to address heterogeneous local conditions across scenarios. We introduce Collaborative Agent Prompts that capture agent-specific collaborative

Table 1. Performance comparison on DAIR-V2X across different labeled data ratios (1%-20%). The baseline model CoAlign [30] is pre-trained on OPV2V and adapted to DAIR-V2X. Blue and red denote the optimal and sub-optimal performances respectively.

Method	1%	2%	5%	10%	20%	Parameter
	AP@50/70	AP@50/70	AP@50/70	AP@50/70	AP@50/70	
None	0.429/0.217	0.429/0.217	0.429/0.217	0.429/0.217	0.429/0.217	0/12,896,384 = 0.00%
Scratch Training	0.139/0.053	0.199/0.069	0.332/0.137	0.423/0.210	0.599/0.395	12,896,384/12,896,384 = 100.00%
Decoder only	0.432/0.183	0.469/0.228	0.497/0.240	0.515/0.276	0.532/0.292	5,140/12,901,524 = 0.04%
SSF [25]	0.507/0.221	0.513/0.264	0.532/0.285	0.518/0.280	0.567/0.333	5,780/12,902,164 = 0.04%
Adapter [5, 15]	0.315/0.089	0.466/0.199	0.575/0.352	0.579/0.380	0.619/0.409	42,420/12,938,804 = 0.33%
DUSA [20]	-/-	-/-	-/-	0.514/0.340	-/-	14,213,266/14,213,266 = 100.00%
MACP [32]	0.455/0.192	0.513/0.239	0.575/0.362	0.597/0.389	0.623/0.414	43,060/12,939,444 = 0.33%
CoPEFT [39]	0.507/0.268	0.517/0.302	0.596/0.384	0.610/0.418	0.627/0.434	111,270/13,007,654 = 0.86%
FlowAdapt [†]	0.533/0.317	0.576/0.373	0.621/0.437	0.638/0.472	0.667/0.507	95,694/12,992,078 = 0.74%
FlowAdapt	0.561/0.343	0.591/0.400	0.631/0.460	0.659/0.499	0.677/0.523	137,393/13,033,777 = 1.05%

context. These prompts are derived from intra-group feature aggregation rather than random initialization:

$$\mathcal{F}_{\text{prompt}} = \phi_{\text{proj}}(\text{Mean}(\{\mathcal{F}_i^{\text{early}} \mid i \in \text{Group}_g\})), \quad (11)$$

where $\mathcal{F}_{\text{prompt}}$ represents prompt features for agent group g , and ϕ_{proj} is a lightweight projection. These prompts are appended to feature sequences during fusion, providing agent-specific guidance without significant overhead. Our implementation incorporate dual-path adapters that learn common domain structure with prompts that specialize to local shifts, forming a cohesive adaptation pipeline.

4. Experiments

4.1. Datasets

We conduct comprehensive experiments on three widely-adopted benchmarks for collaborative perception: OPV2V, DAIR-V2X, and V2XSet [12, 37]. OPV2V [45] is a large-scale vehicle-to-vehicle simulation dataset co-simulated by CARLA [10] and OpenCDA [42], comprising 11,464 frames with 232K annotated 3D bounding boxes from 8 towns across 70+ scenarios, where each frame involves 2-7 agents with an average of 3 per scene. DAIR-V2X [49] is the first real-world vehicle-to-infrastructure dataset containing approximately 9K cooperative frames with synchronized LiDAR from one vehicle and one roadside infrastructure captured in urban traffic, presenting greater challenges due to sensor noise, calibration errors, and temporal asynchronization. V2XSet [44] is a vehicle-to-everything simulation dataset co-generated by CARLA and OpenCDA, containing 11K annotated frames with both vehicle-to-vehicle and vehicle-to-infrastructure perspectives. We follow experimental configurations from recent works [30] and utilize supplementary 3D annotations for DAIR-V2X [40].

4.2. Implementation Details

Evaluation Metrics. We adopt Average Precision (AP) at Intersection-over-Union (IoU) thresholds of 0.5 and 0.7, de-

noted as AP@50 and AP@70, as evaluation metrics for collaborative 3D object detection. We set the evaluation region to $x \in [-100m, 100m]$ and $y \in [-40m, 40m]$ across all datasets. To evaluate robustness under localization uncertainty, we inject Gaussian noise into transformation matrices, where σ_p and σ_y denote the standard deviations for position (in meters) and yaw angle (in degrees), respectively.

Training Configuration. We implement our method using PyTorch on a single NVIDIA RTX 4080 GPU with 16GB VRAM. We pre-train the collaborative perception models on the source dataset using the CoAlign framework [30], where the point clouds are voxelized with a grid size of 0.4×0.4 m. Unless otherwise specified, we conduct parameter-efficient fine-tuning by adapting from OPV2V (source domain) to DAIR-V2X (target domain) using 10% of labeled target samples by default. For reference, the unsupervised domain adaptation baseline DUSA [20] requires 100% unlabeled target data to achieve competitive performance. We freeze backbone parameters and only update the adapter modules and task-specific decoder components. More implementation details are shown in the **Appendix**.

4.3. Quantitative Evaluation

Adaptation from OPV2V to DAIR-V2X. Table 1 evaluates adaptation performance across different labeled data ratios (1%-20%). Direct deployment without adaptation reveals substantial sim-to-real domain gaps, while training from scratch suffers from severe overfitting under limited samples. FlowAdapt consistently achieves superior performance across all data regimes with around 1% trainable parameters. At the 10% labeled data setting, FlowAdapt significantly outperforms CoPEFT, the state-of-the-art PEFT method, by 4.9% and 8.1% in AP@50 and AP@70 respectively. The performance gains become more pronounced under extremely limited data conditions (1%-5%), demonstrating that effective elimination of sample redundancy and recovery of semantic information enable better utilization of scarce labeled samples. In comparison, the un-

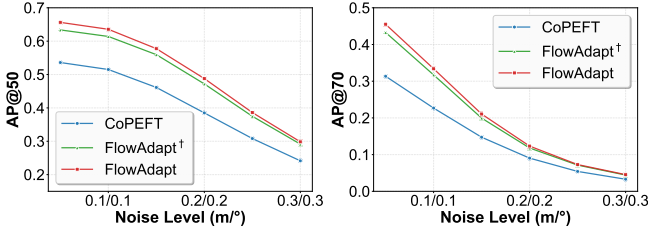


Figure 5. Performance comparison under different localization noise levels when adapting from OPV2V to DAIR-V2X.

supervised baseline DUSA requires 100% unlabeled target data and updates all parameters to achieve competitive performance, making it impractical for label-constrained scenarios. Furthermore, FlowAdapt † , a lightweight variant with 30% fewer trainable parameters than FlowAdapt, maintains strong performance while offering enhanced efficiency. These results highlight FlowAdapt’s effectiveness in bridging sim-to-real gaps with exceptional parameter efficiency and robust adaptation under limited supervision.

Robustness to Pose Noise. Figure 5 evaluates robustness under varying localization noise levels (σ_p/σ_y from $0.1\text{m}/0.1^\circ$ to $0.3\text{m}/0.3^\circ$) on DAIR-V2X. FlowAdapt consistently outperforms CoPEFT across all noise conditions. Under mild noise ($0.1/0.1$), FlowAdapt demonstrates substantial performance advantages in both AP@50 and AP@70 metrics. As noise intensity escalates, all methods experience performance degradation due to increased spatial misalignment between agents. However, FlowAdapt maintains superior robustness—the performance gap between FlowAdapt and CoPEFT remains relatively stable across noise levels, indicating that our method provides consistent benefits even under severe localization uncertainty. This enhanced robustness stems from progressive knowledge transfer, which enables the model to learn semantic patterns less sensitive to spatial perturbations. Notably, FlowAdapt † , the lightweight variant with 30% fewer parameters, closely tracks FlowAdapt’s performance across noise levels, demonstrating strong resilience while offering improved efficiency. These results validate that FlowAdapt not only achieves effective cross-domain adaptation but also enhances robustness to localization uncertainty, essential for reliable deployment in real-world collaborative perception.

Generalization to Different Architectures and Domains. Table 2 evaluates the generalization capability of FlowAdapt across different pre-trained models and target domains. For the AttFuse scenario adapting from OPV2V to DAIR-V2X, FlowAdapt achieves 0.638/0.485, substantially outperforming CoPEFT and other baselines. This demonstrates that FlowAdapt effectively generalizes beyond the CoAlign architecture and maintains strong adaptation capability. For the V2XSet scenario transferring from OPV2V with CoAlign to a different target domain, FlowAdapt achieves 0.934/0.859, showing consistent im-

Table 2. Generalization evaluation across different settings. **Left:** Different fusion (AttFuse as base model adapted from OPV2V to DAIR-V2X). **Right:** Different target domain (CoAlign is used as base model adapted from OPV2V to V2XSet).

Method	Fusion	Target Domain
	AP@50/70	AP@50/70
None	0.442/0.203	0.918/0.839
Scratch Training	0.326/0.167	0.871/0.699
Adapter [5, 15]	0.552/0.359	0.928/0.849
DUSA [20]	0.457/0.324	0.889/0.842
MACP [32]	0.533/0.350	0.930/0.851
CoPEFT [39]	0.554/0.374	0.933/0.854
FlowAdapt	0.638/0.485	0.934/0.859

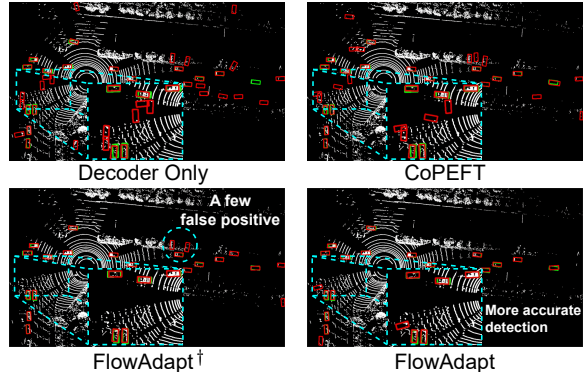


Figure 6. Qualitative comparison of detection results on DAIR-V2X adapted from OPV2V. Green and red 3D bounding boxes represent ground truth and predictions, respectively.

provements over baselines. The smaller performance gap on V2XSet is expected, as both source and target are simulation datasets with similar distributions, resulting in less challenging domain shift compared to sim-to-real transfer. These results validate that FlowAdapt generalizes effectively across diverse collaborative perception architectures and adaptation scenarios with varying domain complexity.

4.4. Qualitative Evaluation

Figure 6 provides qualitative visualization comparing FlowAdapt with baseline methods in cross-domain collaborative perception. The Decoder-only baseline exhibits numerous false positives and missed detections, indicating severe domain gap. CoPEFT shows improved performance but still produces several inaccurate predictions. In the highlighted region, FlowAdapt † demonstrates substantial improvements over baselines but still contains a few false positive detections. In contrast, FlowAdapt achieves the most accurate detection results, successfully eliminating false positives while maintaining precise localization. The visualization aligns with quantitative results in Table 1, validating that FlowAdapt effectively bridges the sim-to-real domain gap through parameter-efficient adaptation.

Table 3. Ablation study on major components of FlowAdapt.

WGS	KTPro	AP@50	AP@70
-	-	0.431	0.227
✓	-	0.456	0.262
-	✓	0.551	0.407
✓	✓	0.659	0.499

Table 4. Ablation study on stage-wise adaptation and progressive knowledge transfer. E/M/L denote adaptation modules at Early/Middle/Late stages respectively, and M+KT/L+KT indicate knowledge transfer from early to middle or late stages.

E	M	L	M+KT	L+KT	AP@50	AP@70
-	-	-	-	-	0.456	0.262
✓	-	-	-	-	0.636	0.458
✓	✓	-	-	-	0.639	0.464
✓	✓	✓	-	-	0.646	0.479
✓	✓	✓	✓	-	0.649	0.492
✓	✓	✓	✓	✓	0.659	0.499

4.5. Ablation Study

Effectiveness of Major Components. Table 3 validates the effectiveness of FlowAdapt’s two core components through ablation study on DAIR-V2X with 10% labeled data. The baseline with only decoder fine-tuning achieves 0.431/0.227 AP@50/70. Incorporating only WGS improves performance to 0.456/0.262, demonstrating that sample selection enhances adaptation quality without architectural modifications. Applying only KTPro yields substantially higher performance at 0.551/0.407, validating that progressive knowledge transfer is crucial for recovering semantic information under parameter-constrained adaptation. The complete FlowAdapt framework achieves 0.659/0.499, significantly outperforming both individual components. This synergy arises because WGS provides high-quality samples with reduced redundancy, enabling KTPro to learn robust knowledge pathways. Conversely, KTPro’s enhanced representations allow better utilization of curated samples from WGS, forming a mutually reinforcing adaptation mechanism.

Effectiveness of Multi-Stage Adaptation and Knowledge Transfer. Table 4 evaluates the contribution of each stage and progressive knowledge transfer, with all configurations including WGS. Without adaptation modules, the framework shows poor performance. Adding early-stage adaptation substantially improves results, validating that adapting features after voxelization is crucial for capturing domain-specific representations. Progressively incorporating middle and late stages yields modest incremental gains, indicating limited improvement without cross-stage information flow. Introducing knowledge transfer fundamentally changes this: middle-stage transfer brings notable improvements, while further enabling late-stage transfer achieves

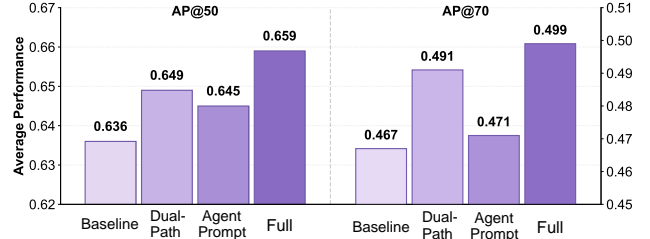


Figure 7. Ablation study on key design decisions of FlowAdapt.

optimal performance. This clearly validates that semantic information is progressively lost in deeper frozen layers, and transferring compressed early-stage representations effectively recovers this information. These results demonstrate that progressive knowledge transfer is essential. Without it, additional stages provide minimal benefits; with proper cross-stage pathways, later stages leverage early-stage features to enhance adaptation quality.

Effectiveness of Key Design Decisions. Figure 7 evaluates the architectural design decisions within FlowAdapt. Without both components, the framework achieves 0.636/0.467 AP@50/70 using only WGS and KTPro. Incorporating Dual-Path Adapter alone improves performance to 0.649/0.491, demonstrating that complementary spatial and channel processing effectively captures diverse domain patterns—spatial paths handle local geometric variations while channel paths model global semantic dependencies. Adding only Agent Prompts yields 0.645/0.471, validating that agent-specific context from intra-group aggregation provides valuable fine-grained adaptation for heterogeneous collaborative scenarios. The complete configuration achieves 0.659/0.499, outperforming individual components. This synergy arises from their hierarchical roles: Dual-Path Adapter establishes a robust shared feature space for domain-level adaptation, while Agent Prompts inject instance-specific refinements for agent-level variations. Together, they enable FlowAdapt to handle both global domain shifts and local collaborative heterogeneity.

5. Conclusion

In this paper, we revisit PEFT adaptation for collaborative perception from an optimal-transport perspective and present FlowAdapt, a parameter-efficient framework that couples Wasserstein Greedy Sampling strategy and Progressive Knowledge Transfer module. These proposed components significantly reduces inter-frame redundancy while preserving fine-grained semantics in deep layers, and achieves state-of-the-art adaptation performance with only 1% trainable parameters across multiple benchmarks. Experimental results verify consistent gains in accuracy and robustness under domain shifts. In the future, we will extend FlowAdapt to multi-modal fusion pipelines, integrate more physical constraints into the transport objective to further improve reliability in open-world deployment.

References

[1] Martin Arjovsky, Soumith Chintala, and Léon Bottou. Wasserstein gan, 2017. 3

[2] Antoine Caillot, Safa Ouerghi, Pascal Vasseur, Rémi Bouteau, and Yohan Dupuis. Survey on cooperative perception in an automotive context. *IEEE Transactions on Intelligent Transportation Systems*, 23(9):14204–14223, 2022. 1

[3] Qi Chen. F-cooper: Feature based cooperative perception for autonomous vehicle edge computing system using 3D point clouds, 2019. 1, 2

[4] Qi Chen, Sihai Tang, Qing Yang, and Song Fu. Cooper: Cooperative perception for connected autonomous vehicles based on 3d point clouds. In *2019 IEEE 39th International Conference on Distributed Computing Systems (ICDCS)*, pages 514–524, 2019. 2

[5] Shoufa Chen, Chongjian Ge, Zhan Tong, Jiangliu Wang, Yibing Song, Jue Wang, and Ping Luo. Adaptformer: Adapting vision transformers for scalable visual recognition, 2022. 3, 6, 7

[6] Nicolas Courty, Rémi Flamary, Devis Tuia, and Alain Rakotomamonjy. Optimal transport for domain adaptation, 2016. 3

[7] Nicolas Courty, Rémi Flamary, Amaury Habrard, and Alain Rakotomamonjy. Joint distribution optimal transportation for domain adaptation, 2017. 3

[8] Xiao Cui, Mo Zhu, Yulei Qin, Liang Xie, Wengang Zhou, and Houqiang Li. Multi-level optimal transport for universal cross-tokenizer knowledge distillation on language models, 2025. 3

[9] Tim Dettmers, Artidoro Pagnoni, Ari Holtzman, and Luke Zettlemoyer. Qlora: Efficient finetuning of quantized llms, 2023. 3

[10] Alexey Dosovitskiy, German Ros, Felipe Codevilla, Antonio Lopez, and Vladlen Koltun. Carla: An open urban driving simulator, 2017. 6

[11] Teofilo F. Gonzalez. Clustering to minimize the maximum intercluster distance. *Theoretical Computer Science*, 38: 293–306, 1985. 4

[12] Yushan Han, Hui Zhang, Huifang Li, Yi Jin, Congyan Lang, and Yidong Li. Collaborative perception in autonomous driving: Methods, datasets, and challenges. *IEEE Intelligent Transportation Systems Magazine*, 15(6):131–151, 2023. 6

[13] Zeyu Han, Chao Gao, Jinyang Liu, Jeff Zhang, and Sai Qian Zhang. Parameter-efficient fine-tuning for large models: A comprehensive survey, 2024. 3

[14] Haoyu He, Jianfei Cai, Jing Zhang, Dacheng Tao, and Bohan Zhuang. Sensitivity-aware visual parameter-efficient fine-tuning, 2023. 1

[15] Neil Houlsby, Andrei Giurgiu, Stanislaw Jastrzebski, Bruna Morrone, Quentin de Laroussilhe, Andrea Gesmundo, Mona Attariyan, and Sylvain Gelly. Parameter-efficient transfer learning for nlp, 2019. 1, 3, 6, 7

[16] Edward J. Hu, Yelong Shen, Phillip Wallis, Zeyuan Allen-Zhu, Yuanzhi Li, Shean Wang, Lu Wang, and Weizhu Chen. Lora: Low-rank adaptation of large language models, 2021. 1, 3

[17] Yue Hu, Shaoheng Fang, Zixing Lei, Yiqi Zhong, and Si-heng Chen. Where2comm: Communication-efficient collaborative perception via spatial confidence maps, 2022. 2

[18] Tao Huang, Jianan Liu, Xi Zhou, Dinh C. Nguyen, Mostafa Rahimi Azghadi, Yuxuan Xia, Qing-Long Han, and Sumei Sun. V2X Cooperative Perception for Autonomous Driving: Recent Advances and Challenges, 2024. 1

[19] Menglin Jia, Luming Tang, Bor-Chun Chen, Claire Cardie, Serge Belongie, Bharath Hariharan, and Ser-Nam Lim. Visual prompt tuning, 2022. 3

[20] Xianghao Kong, Wentao Jiang, Jinrang Jia, Yifeng Shi, Runsheng Xu, and Si Liu. DUSA: Decoupled unsupervised Sim2Real adaptation for vehicle-to-everything collaborative perception. In *Proceedings of the 31st ACM International Conference on Multimedia*, pages 1943–1954, 2023. 6, 7

[21] Zixing Lei, Zhenyang Ni, Ruize Han, Shuo Tang, Dingju Wang, Chen Feng, Siheng Chen, and Yanfeng Wang. Robust collaborative perception without external localization and clock devices, 2024. 2

[22] Xiang Lisa Li and Percy Liang. Prefix-tuning: Optimizing continuous prompts for generation, 2021. 3

[23] Yiming Li, Shunli Ren, Pengxiang Wu, Siheng Chen, Chen Feng, and Wenjun Zhang. Learning distilled collaboration graph for multi-agent perception, 2022. 2

[24] Vladislav Lalin, Vijeta Deshpande, Xiaowei Yao, and Anna Rumshisky. Scaling down to scale up: A guide to parameter-efficient fine-tuning, 2024. 3

[25] Dongze Lian, Daquan Zhou, Jiashi Feng, and Xinchao Wang. Scaling & shifting your features: A new baseline for efficient model tuning, 2023. 6

[26] Si Liu, Chen Gao, Yuan Chen, Xingyu Peng, Xianghao Kong, Kun Wang, Runsheng Xu, Wentao Jiang, Hao Xiang, Jiaqi Ma, and Miao Wang. Towards vehicle-to-everything autonomous driving: A survey on collaborative perception, 2023. 2

[27] Shih-Yang Liu, Chien-Yi Wang, Hongxu Yin, Pavlo Molchanov, Yu-Chiang Frank Wang, Kwang-Ting Cheng, and Min-Hung Chen. Dora: Weight-decomposed low-rank adaptation, 2024. 3

[28] Yen-Cheng Liu, Junjiao Tian, Nathaniel Glaser, and Zsolt Kira. When2com: Multi-Agent Perception via Communication Graph Grouping. In *2020 IEEE/CVF Conference on Computer Vision and Pattern Recognition (CVPR)*, pages 4105–4114, Seattle, WA, USA, 2020. IEEE. 2

[29] Yen-Cheng Liu, Junjiao Tian, Chih-Yao Ma, Nathan Glaser, Chia-Wen Kuo, and Zsolt Kira. Who2com: Collaborative perception via learnable handshake communication, 2020. 2

[30] Yifan Lu, Quanhao Li, Baoan Liu, Mehrdad Dianati, Chen Feng, Siheng Chen, and Yanfeng Wang. Robust collaborative 3D object detection in presence of pose errors, 2023. 2, 6

[31] Yifan Lu, Yue Hu, Yiqi Zhong, Dequan Wang, Yanfeng Wang, and Siheng Chen. An extensible framework for open heterogeneous collaborative perception, 2024. 1, 2

[32] Yunsheng Ma, Juanwu Lu, Can Cui, Sicheng Zhao, Xu Cao, Wenqian Ye, and Ziran Wang. MACP: Efficient model adaptation for cooperative perception. In *2024 IEEE/CVF Winter Conference on Applications of Computer Vision (WACV)*, 2024. 1

pages 3361–3370, Waikoloa, HI, USA, 2024. IEEE. 1, 3, 6, 7

[33] Tiehua Mei, Hengrui Chen, Peng Yu, Jiaqing Liang, and Deqing Yang. Goracs: Group-level optimal transport-guided coreset selection for llm-based recommender systems, 2025. 3

[34] Gabriel Peyré and Marco Cuturi. Computational optimal transport, 2020. 2, 3

[35] Andreas Rauch, Felix Klanner, Ralph Rasshofer, and Klaus Dietmayer. Car2x-based perception in a high-level fusion architecture for cooperative perception systems. In *2012 IEEE Intelligent Vehicles Symposium*, pages 270–275, 2012. 2

[36] Zhiying Song, Lei Yang, Fuxi Wen, and Jun Li. TraF-align: Trajectory-aware feature alignment for asynchronous multi-agent perception, 2025. 1, 2

[37] Naibang Wang, Deyong Shang, Yan Gong, Xiaoxi Hu, Ziyi Song, Lei Yang, Yuhua Huang, Xiaoyu Wang, and Jianlu Lu. Collaborative perception datasets for autonomous driving: A review, 2025. 6

[38] Tsun-Hsuan Wang, Sivabalan Manivasagam, Ming Liang, Bin Yang, Wenyuan Zeng, and Raquel Urtasun. V2VNet: Vehicle-to-vehicle communication for joint perception and prediction. In *Computer Vision – ECCV 2020*, pages 605–621. Springer International Publishing, Cham, 2020. 2

[39] Quanmin Wei, Penglin Dai, Wei Li, Bingyi Liu, and Xiao Wu. CoPEFT: Fast adaptation framework for multi-agent collaborative perception with parameter-efficient fine-tuning, 2025. 1, 2, 3, 6, 7

[40] Li Xiang, Junbo Yin, Wei Li, Cheng-Zhong Xu, Ruigang Yang, and Jianbing Shen. Di-v2x: Learning domain-invariant representation for vehicle-infrastructure collaborative 3d object detection, 2023. 6

[41] Yi Xin, Jianjiang Yang, Siqi Luo, Yuntao Du, Qi Qin, Kangrui Cen, Yangfan He, Zhiwei Zhang, Bin Fu, Xiaokang Yang, Guangtao Zhai, Ming-Hsuan Yang, and Xiaohong Liu. Parameter-efficient fine-tuning for pre-trained vision models: A survey and benchmark, 2025. 1

[42] Runsheng Xu, Yi Guo, Xu Han, Xin Xia, Hao Xiang, and Jiaqi Ma. Opencda:an open cooperative driving automation framework integrated with co-simulation, 2021. 6

[43] Runsheng Xu, Zhengzhong Tu, Hao Xiang, Wei Shao, Bolei Zhou, and Jiaqi Ma. Cobevt: Cooperative bird’s eye view semantic segmentation with sparse transformers, 2022. 2

[44] Runsheng Xu, Hao Xiang, Zhengzhong Tu, Xin Xia, Ming-Hsuan Yang, and Jiaqi Ma. V2X-ViT: Vehicle-to-everything cooperative perception with vision transformer. In *Computer Vision – ECCV 2022*, pages 107–124. Springer Nature Switzerland, Cham, 2022. 2, 6

[45] Runsheng Xu, Hao Xiang, Xin Xia, Xu Han, Jinlong Li, and Jiaqi Ma. Opv2v: An open benchmark dataset and fusion pipeline for perception with vehicle-to-vehicle communication, 2022. 6

[46] Runsheng Xu, Chia-Ju Chen, Zhengzhong Tu, and Ming-Hsuan Yang. V2x-vitv2: Improved vision transformers for vehicle-to-everything cooperative perception. *IEEE Transactions on Pattern Analysis and Machine Intelligence*, 47(1):650–662, 2025. 2

[47] Yunjiang Xu, Lingzhi Li, Jin Wang, Benyuan Yang, Zhiwen Wu, Xinhong Chen, and Jianping Wang. Codyntrust: Robust asynchronous collaborative perception via dynamic feature trust modulus, 2025. 2

[48] Kang Yang, Tianci Bu, Lantao Li, Chunxu Li, Yongcai Wang, and Deying Li. Is discretization fusion all you need for collaborative perception?, 2025. 1

[49] Haibao Yu, Yizhen Luo, Mao Shu, Yiyi Huo, Zebang Yang, Yifeng Shi, Zhenglong Guo, Hanyu Li, Xing Hu, Jirui Yuan, and Zaiqing Nie. Dair-v2x: A large-scale dataset for vehicle-infrastructure cooperative 3d object detection. In *2022 IEEE/CVF Conference on Computer Vision and Pattern Recognition (CVPR)*, pages 21329–21338, 2022. 6

[50] Jingyu Zhang, Kun Yang, Yilei Wang, Hanqi Wang, Peng Sun, and Liang Song. ERMVP: Communication-efficient and collaboration-robust multi-vehicle perception in challenging environments. In *2024 IEEE/CVF Conference on Computer Vision and Pattern Recognition (CVPR)*, pages 12575–12584, Seattle, WA, USA, 2024. IEEE. 1, 2

[51] Qingru Zhang, Minshuo Chen, Alexander Bukharin, Nikos Karapatsiakis, Pengcheng He, Yu Cheng, Weizhu Chen, and Tuo Zhao. Adalora: Adaptive budget allocation for parameter-efficient fine-tuning, 2023. 3